

SUPPORTING INFORMATION for

Investigation on the electrochemistry and cytotoxicity of the natural product marcanine A and its synthetic derivatives

Nadine Jacobs, Steffen Lang, Robin Panisch, Gunther Wittstock, Ulrich Groth
and Hamid R. Nasiri*

Contents of SUPPORTING INFORMATION

Electrochemistry	S2
Cell cytotoxicity assay	S13
Density functional calculations	S14
Overview of the multi-step synthesis	S22

SUPPLEMENTARY MATERIALS AND METHODS

Electrochemistry

All used solutions were freshly prepared. Tetrabutylammonium hexafluorophosphate (TBAPF₆, Fluka, Steinheim), silver perchlorate (AgClO₄, Fluka, Steinheim) were used as received. Dimethylformamide (DMF, Carl Roth, Karlsruhe) was refluxed over calcium hydride (CaH₂, Merck, Hohenbrunn) for 30 min then distilled and stored under dry nitrogen.

Cyclovoltammetric (CV) experiments were performed using a conventional three-electrode system cell with 0.1 M tetrabutylammonium hexafluorophosphate (TBAPF₆) / DMF as supporting electrolyte on a platinum disc electrode as working electrode (WE, $d = 1$ mm) and a platinum plate counter electrode (CE, $A = 2$ cm²). The reference electrode was a Haber-Luggin-Dual-Reference electrode¹ (Fig. S1) with 0.01 M AgClO₄|0.1 M TBAPF₆|DMF. The quinones were used in concentrations of 1 mM except compound **8**. Here concentrations of 3.8, 1.9 and 0.95 mM have been used. The solutions of the quinones were deaerated with dry nitrogen prior to use and maintained under dry nitrogen atmosphere. The reversibility of the cyclic voltammograms has been evaluated. All electrochemical experiments were performed at room temperature. The formal potential (E°) was determined using $E^{\circ} = 0.5(E_{pa} + E_{pc})$ for CV experiments. Differential pulse voltammetric experiments were performed under the same conditions and the half wave potential $E_{1/2}$ was determined by plotting the peak potential E_p vs. the pulse height ΔE and extrapolating the pulse height to $\Delta E = 0$. In case that the diffusion coefficients between the oxidized and reduced form do not differ significantly, $E^{\circ} \approx E_{1/2}$.

A CHI660 potentiostat with related software has been used to perform the experiments. The software was also used to determine the peak potentials (E_p) and peak currents (i_p).

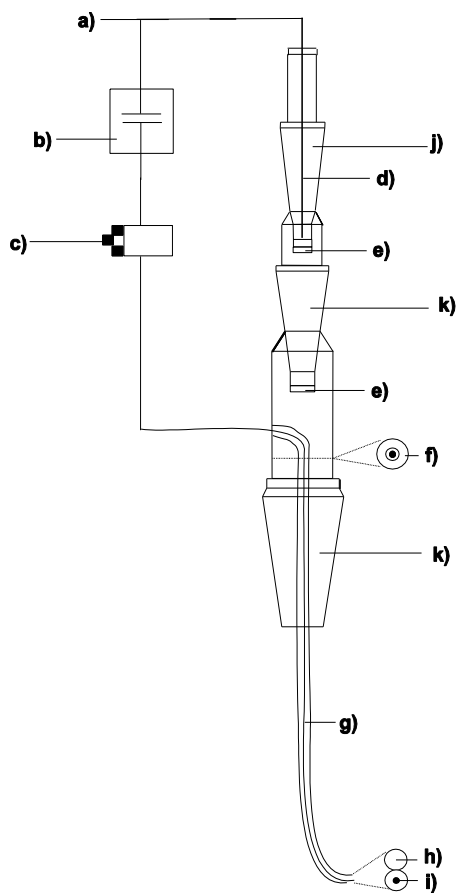


Figure S1. Construction of the Haber-Luggin dual reference electrode according to Gollas et al.¹ a) copper wire, b) capacitor (0.01 μ F), c) clamp, d) silver wire, e) glass frit, f) platinum wire sealed in glass capillary, g) platinum wire, h) tip of the Luggin capillary, i) platinum wire tip, j) 0.01 M AgClO_4 /0.1 M TBAPF_6 in DMF, k) 0.1 M TBAPF_6 in DMF

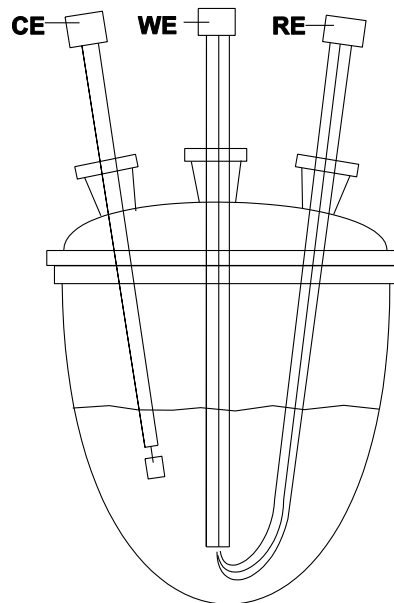


Figure S2. Schematic design of the three electrode cell.

Compound **9** was measured in different concentrations with different scan rates.

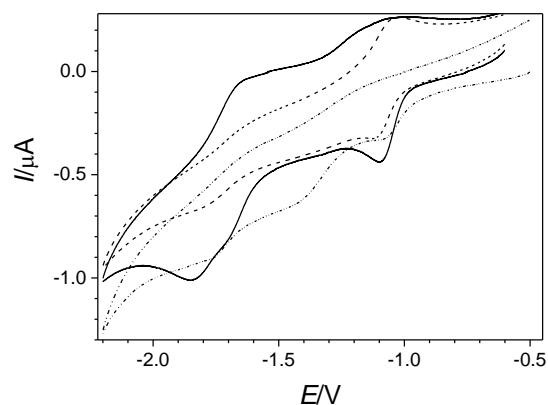


Figure S3. CVs of **9** with different concentrations, $c = 3.8$ mM (solid), $c = 1.9$ mM (dashed), $c = 0.95$ mM (dotted). Scan rate = 0.1 V/s

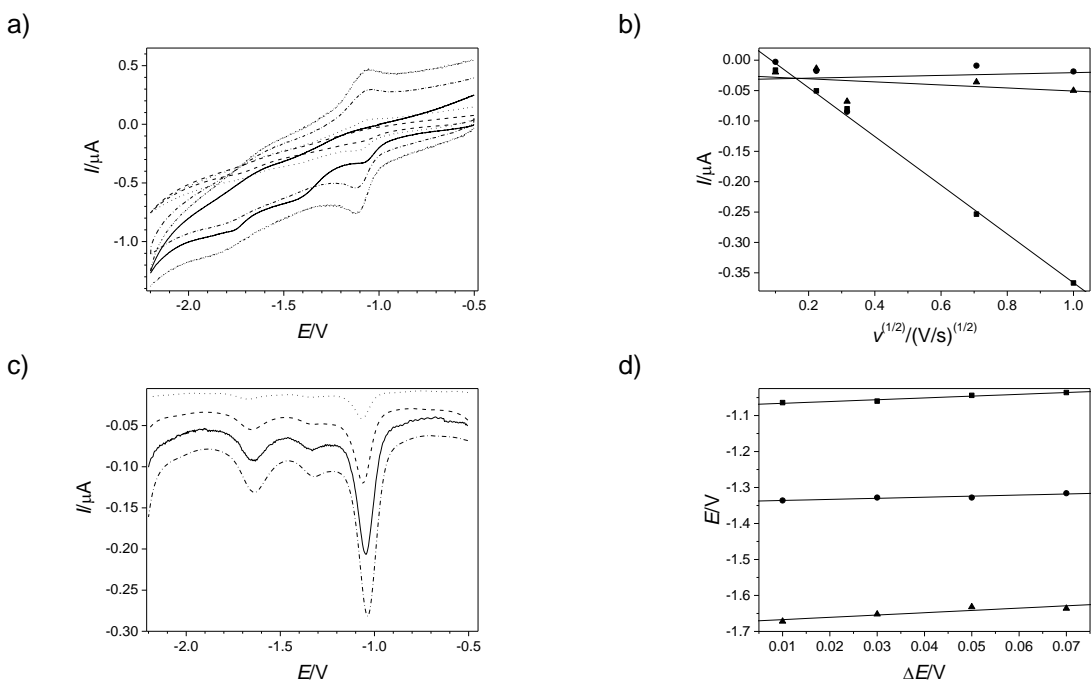


Figure S4. CV of **9** with $c = 0.95$ mM. a) different scan rates (0.1 V/s (solid), 0.01 V/s (dashed), 0.05 V/s (dotted), 0.5 V/s (dash-dot), 1.0 V/s (dash-dot-dot)), b) dependency of anodic peak potential (I_{pa}) on square root of scan rate ($v^{1/2}$) (1st peak (■), 2nd peak (●), 3rd peak (▲)), c) DPV with different pulse heights (0.07 V (dash-dot), 0.05 V (solid), 0.03 V (dashed), 0.01 V (dotted), and d) dependency of peak potential (E_p) on pulse height (ΔE) (1st peak (■), 2nd peak (●), 3rd peak (▲)).

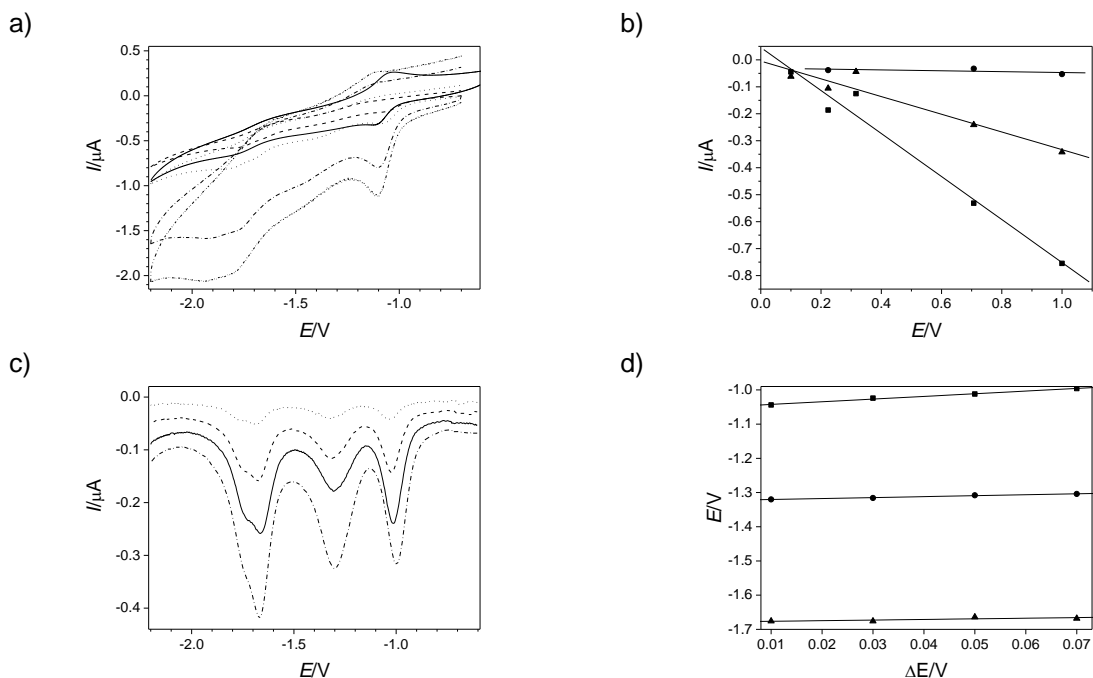


Figure S5. CV of **9** with $c = 1.9$ mM. a) different scan rates (0.01 V/s (dashed), 0.05 V/s (dotted), 0.1 V/s (solid), 0.5 V/s (dash-dot), 1.0 V/s (dash-dot-dot)), b) dependency of anodic peak potential (E_{pa}) on square root of scan rate ($v^{1/2}$) (1st peak (■), 2nd peak (●), 3rd peak (▲)), c) DPV with different pulse heights (0.07 V (dash-dot), 0.05 V (solid), 0.03 V (dashed), 0.01 V (dotted),) and d) dependency of peak potential (E_p) on pulse height (ΔE) (1st peak (■), 2nd peak (●), 3rd peak (▲)).

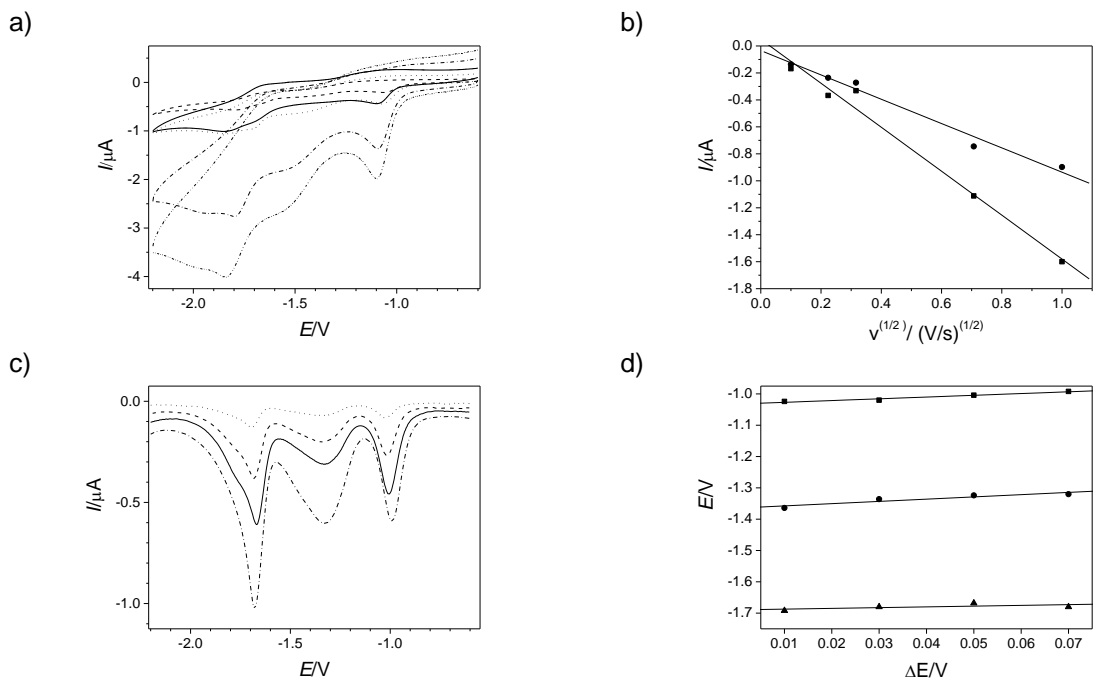


Figure S6. CV of **9** with $c = 3.8$ mM. a) different scan rates (0.01 V/s (dashed), 0.05 V/s (dotted), 0.1 V/s (solid), 0.5 V/s (dash-dot), 1.0 V/s (dash-dot-dot)), b) dependency of anodic peak potential (E_{pa}) on square root of scan rate ($v^{1/2}$) (1st peak (■), 2nd peak (●), 3rd Peak (▲)), c) DPV with different pulse heights (0.07 V (dash-dot), 0.05 V (solid), 0.03 V (dashed), 0.01 V (dotted)) and d)

dependency of peak potential (E_p) on pulse height (ΔE) (1st peak (■), 2nd peak (●), 3rd peak (▲)).

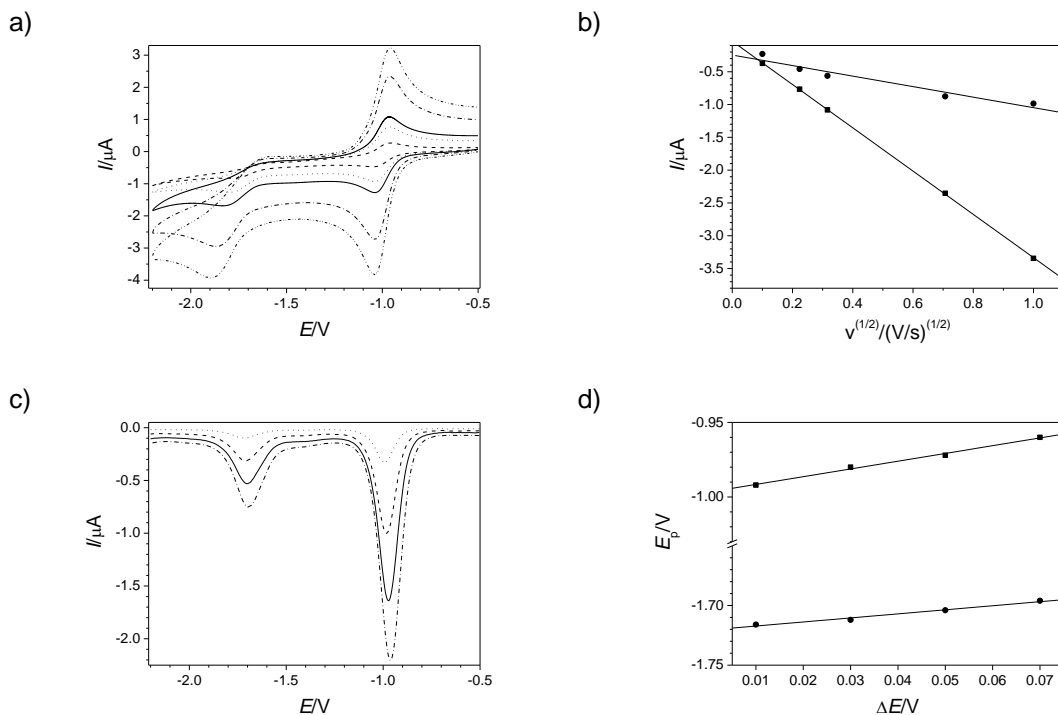


Figure S7. CV of **6** with $c = 1 \text{ mM}$. a) different scanrates (0.01 V/s (dashed), 0.05 V/s (dotted), 0.1 V/s (solid), 0.5 V/s (dash-dot), 1.0 V/s (dash-dot-dot)), b) dependency of anodic peak potential (E_p) on square root of scanrate ($v^{1/2}$) (1st peak (■), 2nd peak (●)), c) DPV with different pulse heights (0.07 V (dash-dot), 0.05 V (solid), 0.03 V (dashed), 0.01 V (dotted)) and d) dependency of peak potential (E_p) on pulse height (ΔE) (1st peak (■), 2nd peak (●)).

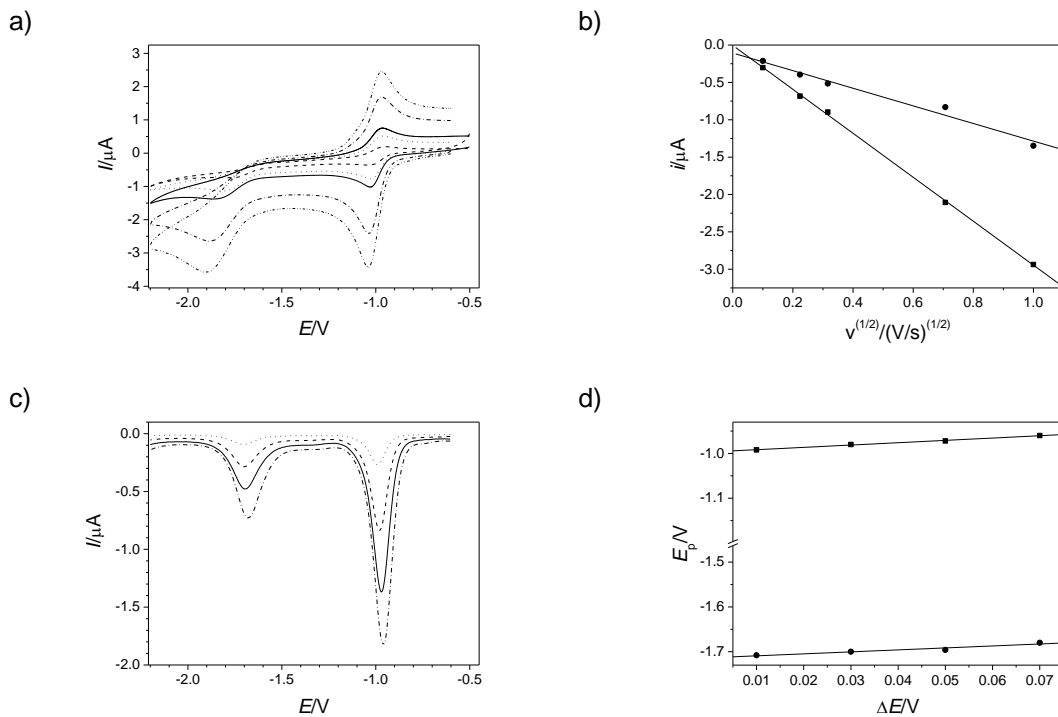


Figure S8. CV of **5** with $c = 1 \text{ mM}$. a) different scan rates (0.01 V/s (dashed), 0.05 V/s (dotted), 0.1 V/s (solid), 0.5 V/s (dash-dot), 1.0 V/s (dash-dot-dot)), b) dependency of anodic peak potential (i_{pa}) on square root of scanrate ($v^{1/2}$) (1st peak (■), 2nd peak (●)), c) DPV with different pulse heights (0.07 V (dash-dot), 0.05 V (solid), 0.03 V (dashed), 0.01 V (dotted)) and d) dependency of peak potential (E_p) on pulse height (ΔE) (1st peak (■), 2nd peak (●)).

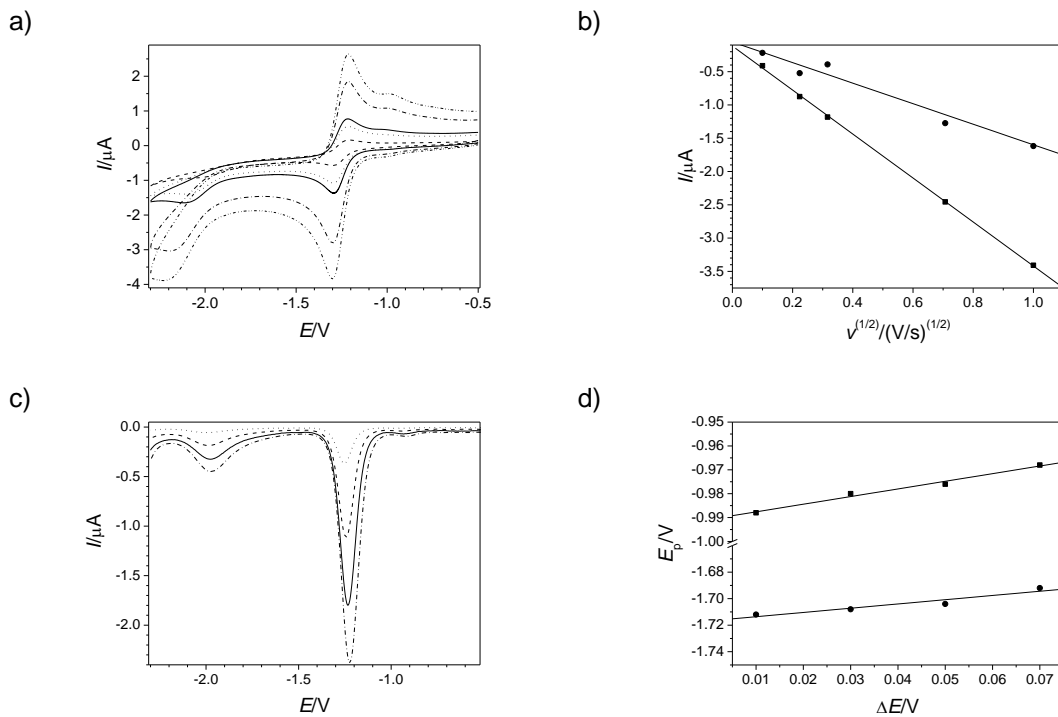


Figure S9. CV of **10** with $c = 1$ mM. a) different scanrates (0.01 V/s (dashed), 0.05 V/s (dotted), 0.1 V/s (solid), 0.5 V/s (dash-dot), 1.0 V/s (dash-dot-dot)), b) dependency of anodic peak potential (E_{pa}) on square root of scan rate ($v^{1/2}$) (1st peak (■), 2nd peak (●)), c) DPV with different pulse heights (0.07 V (dash-dot), 0.05 V (solid), 0.03 V (dashed), 0.01 V (dotted)) and d) dependency of peak potential (E_p) on pulse height (ΔE) (1st peak (■), 2nd peak (●)).

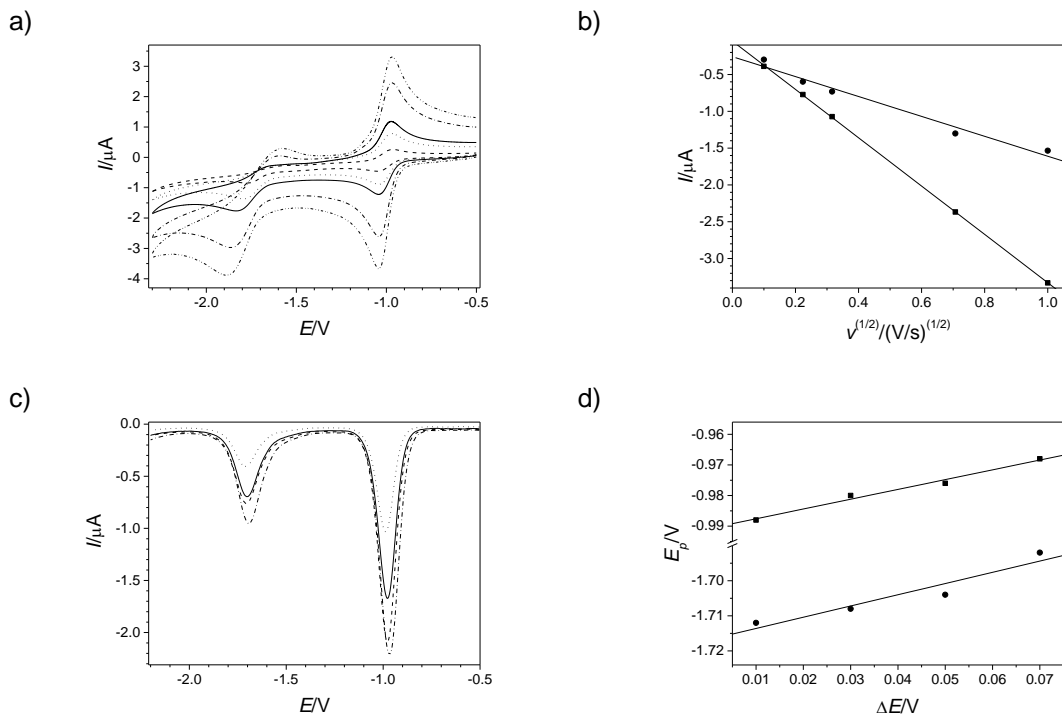


Figure S10. CV of 7 with $c = 1 \text{ mM}$. a) different scan rates (0.01 V/s (dashed), 0.05 V/s (dotted), 0.1 V/s (solid), 0.5 V/s (dash-dot), 1.0 V/s (dash-dot-dot)), b) dependency of anodic peak potential (I_{pa}) on square root of scanrate ($v^{1/2}$) (1st peak (■), 2nd peak (●)), c) DPV with different pulse heights (0.07 V (dash-dot), 0.05 V (solid), 0.03 V (dashed), 0.01 V (dotted)) and d) dependency of peak potential (E_p) on pulse height (ΔE) (1st peak (■), 2nd peak (●)).

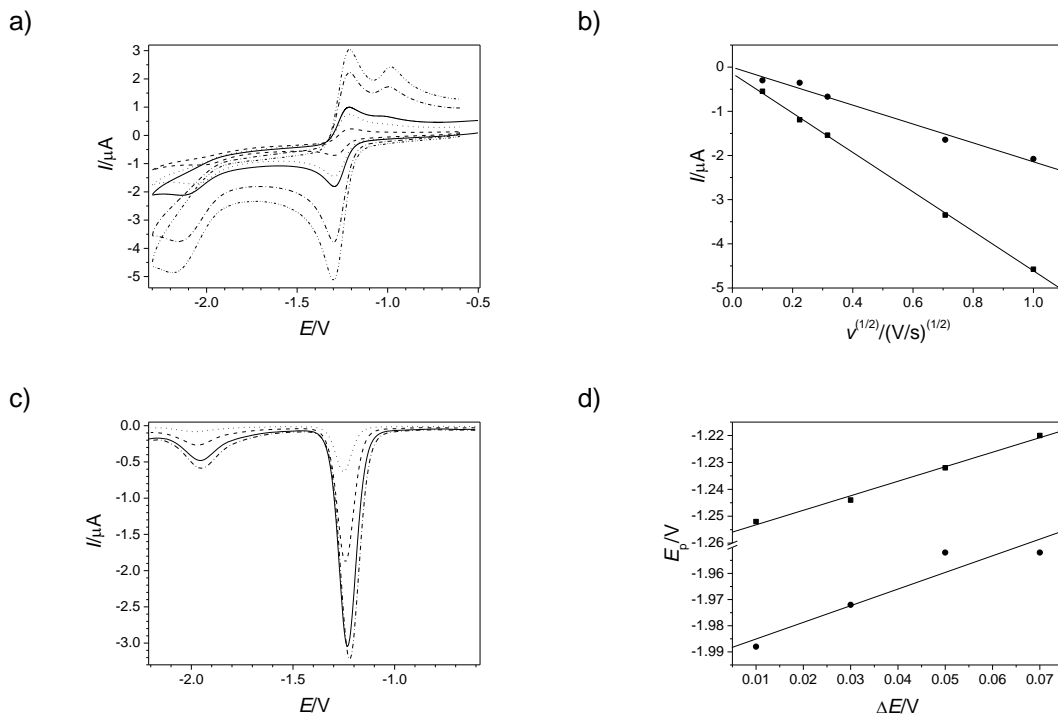


Figure S11. CV of **11** with $c = 1$ mM. a) different scanrates (0.01 V/s (dashed), 0.05 V/s (dotted), 0.1 V/s (solid), 0.5 V/s (dash-dot), 1.0 V/s (dash-dot-dot)), b) dependency of anodic peak potential (I_{pa}) on square root of scanrate ($v^{1/2}$) (1st peak (■), 2nd peak (●)), c) DPV with different pulse heights (0.07 V (dash-dot), 0.05 V (solid), 0.03 V (dashed), 0.01 V (dotted)) and d) dependency of peak potential (E_p) on pulse height (ΔE) (1st peak (■), 2nd peak (●)).

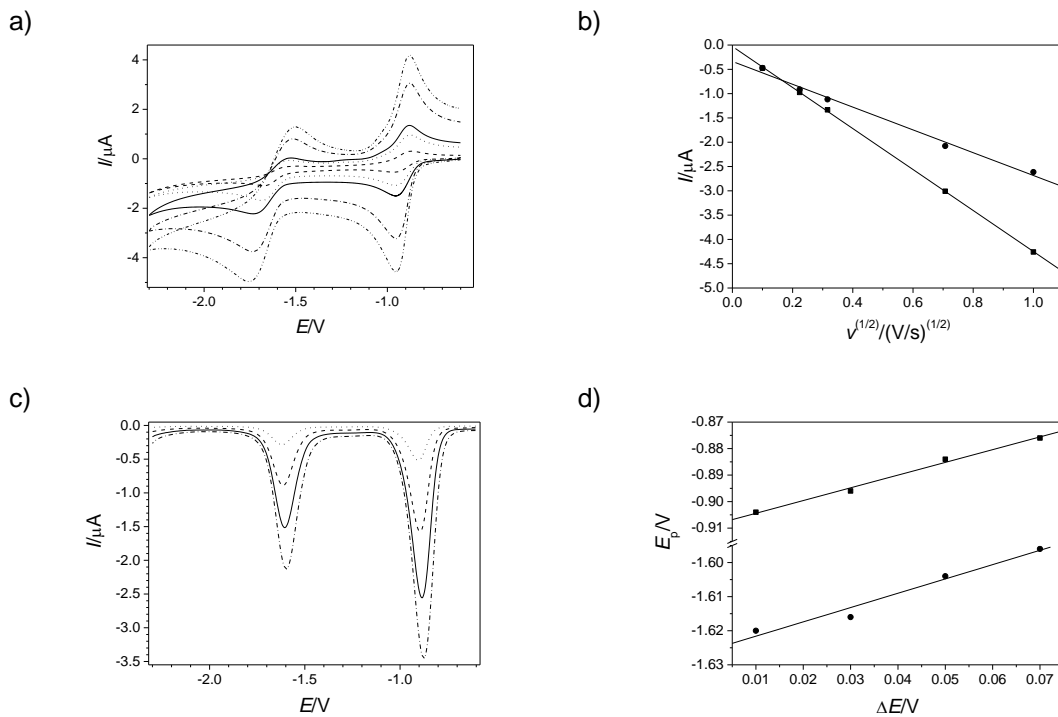


Figure S12. CV of **8** with $c = 1 \text{ mM}$. a) different scan rates (0.01 V/s (dashed), 0.05 V/s (dotted), 0.1 V/s (solid), 0.5 V/s (dash-dot), 1.0 V/s (dash-dot-dot)), b) dependency of anodic peak potential (I_{pa}) on square root of scanrate ($v^{1/2}$) (1st peak (■), 2nd peak (●)), c) DPV with different pulse heights (0.07 V (dash-dot), 0.05 V (solid), 0.03 V (dashed), 0.01 V (dotted)) and d) dependency of peak potential (E_p) on pulse height (ΔE) (1st peak (■), 2nd peak (●)).

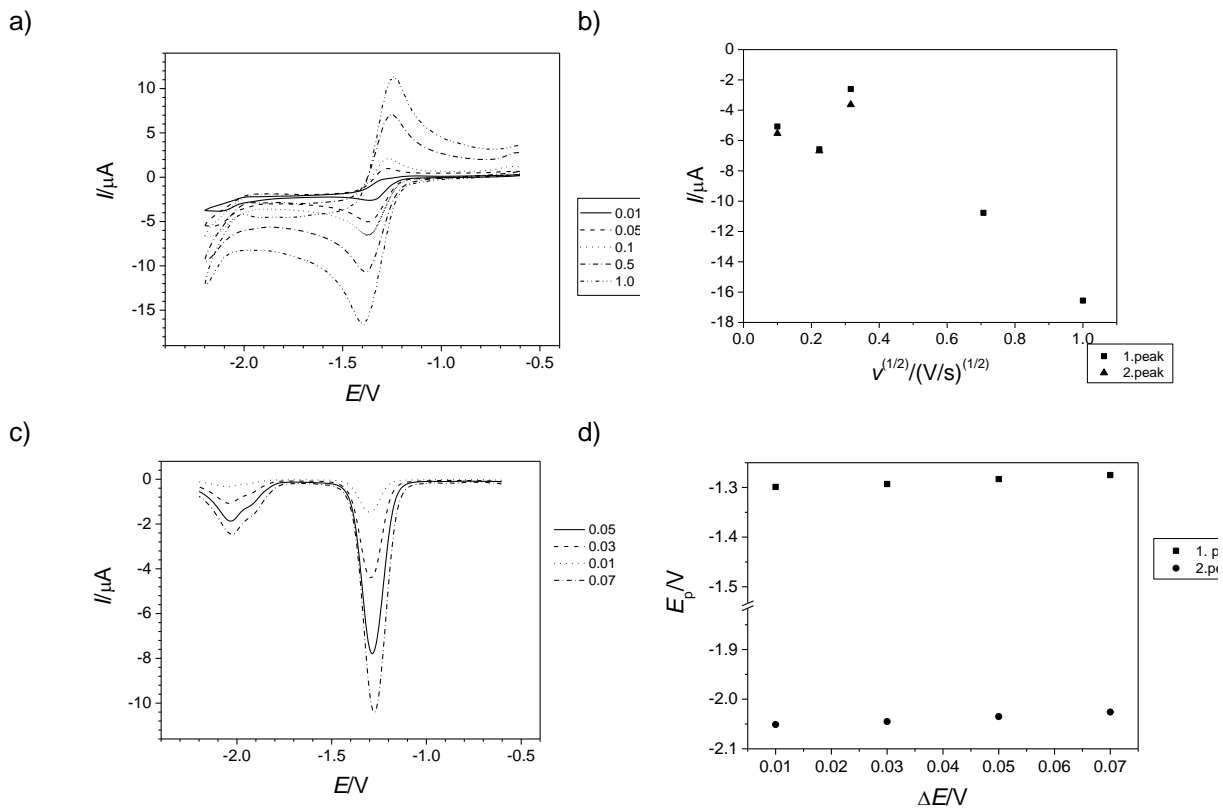


Figure S13. CV of **12** with $c = 1 \text{ mM}$. a) different scan rates (0.01 V/s (dashed), 0.05 V/s (dotted), 0.1 V/s (solid), 0.5 V/s (dash-dot), 1.0 V/s (dash-dot-dot)), b) dependency of anodic peak potential (I_{pa}) on square root of scanrate ($v^{1/2}$) (1st peak (■), 2nd peak (●)), c) DPV with different pulse heights (0.07 V (dash-dot), 0.05 V (solid), 0.03 V (dashed), 0.01 V (dotted)) and d) dependency of peak potential (E_p) on pulse height (ΔE) (1st peak (■), 2nd peak (●)).

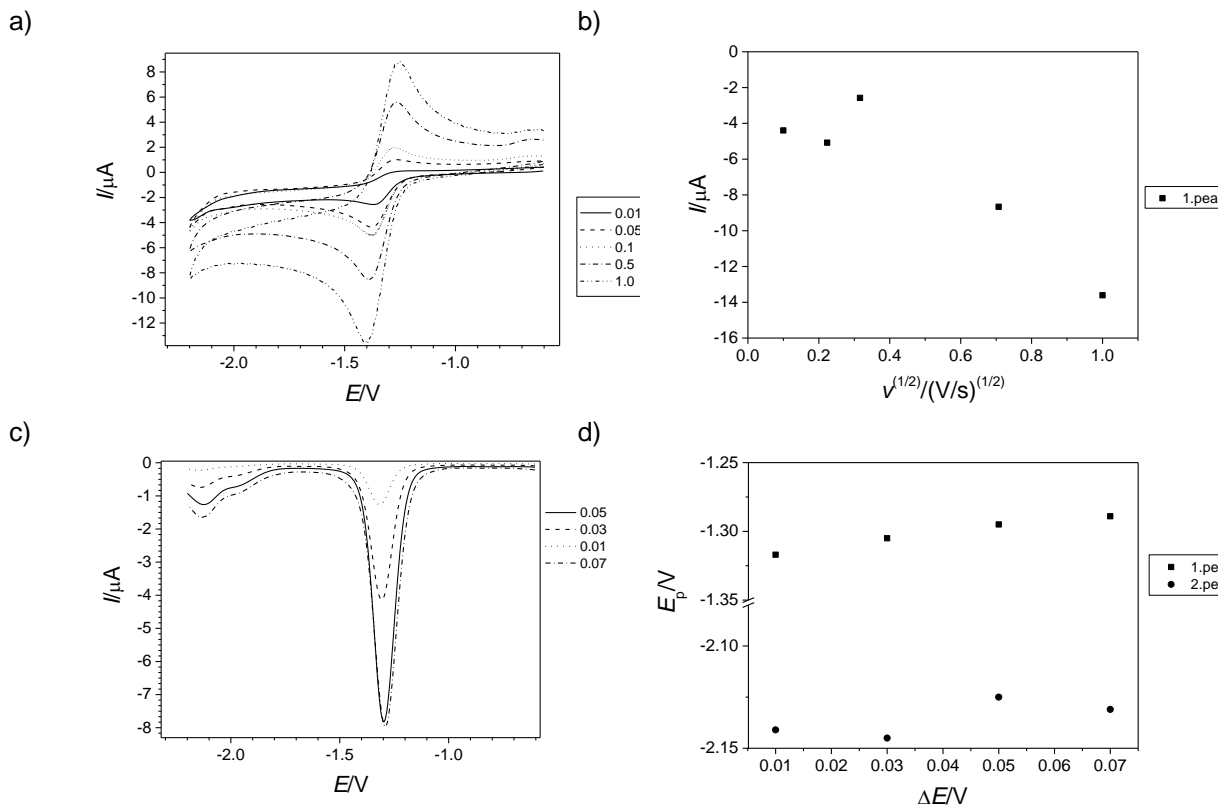


Figure S14. CV of **13** with $c = 1$ mM. a) different scan rates (0.01 V/s (dashed), 0.05 V/s (dotted), 0.1 V/s (solid), 0.5 V/s (dash-dot), 1.0 V/s (dash-dot-dot)), b) dependency of anodic peak potential (E_{pa}) on square root of scanrate ($v^{1/2}$) (1st peak (■), 2nd peak (●)), c) DPV with different pulse heights (0.07 V (dash-dot), 0.05 V (solid), 0.03 V (dashed), 0.01 V (dotted)) and d) dependency of peak potential (E_p) on pulse height (ΔE) (1st peak (■), 2nd peak (●)).

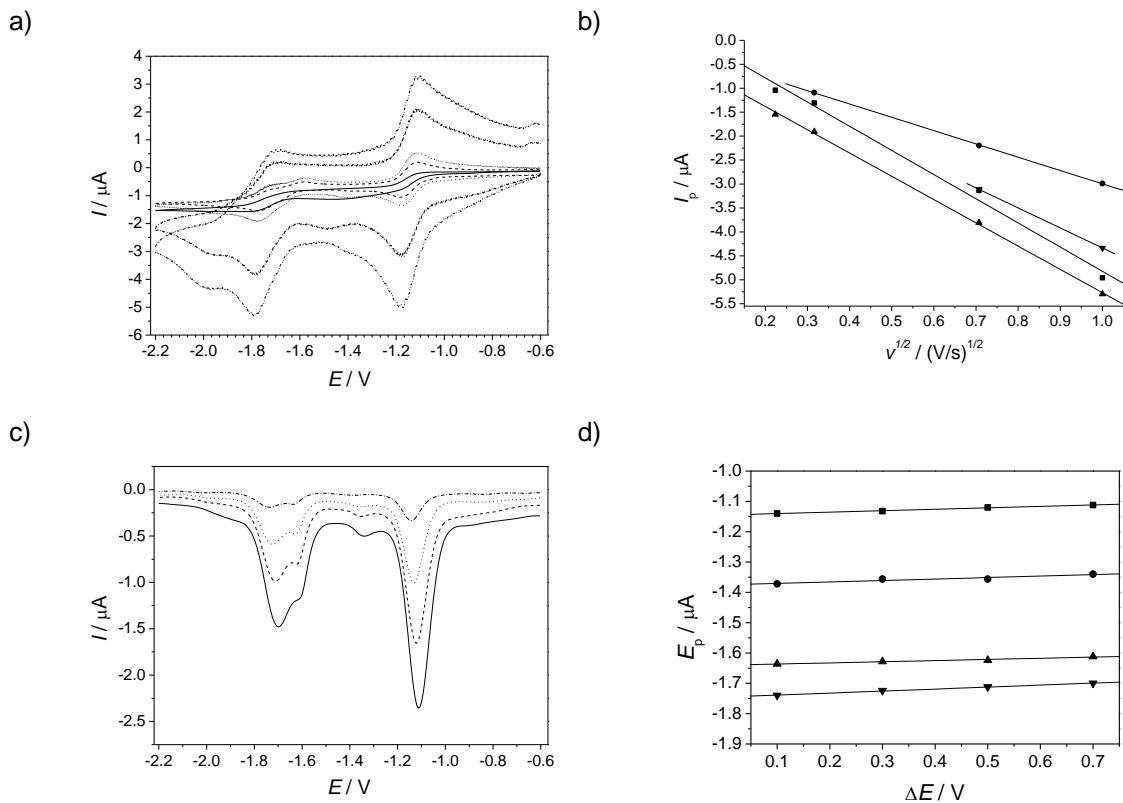


Figure S15. CV of **14** with $c = 1 \text{ mM}$. a) different scan rates (0.01 V/s (solid), 0.05 V/s (dashed), 0.1 V/s (dotted), 0.5 V/s (dash-dot), 1.0 V/s (dash-dot-dot)), b) dependency of anodic peak potential (I_{pa}) on square root of scanrate ($v^{1/2}$) (1st peak (■), 2nd peak (●), 3rd peak (▲), 4th peak (▼)), c) DPV with different pulse heights (0.07 V (dash-dot), 0.05 V (solid), 0.03 V (dashed), 0.01 V (dotted)) and d) dependency of peak potential (E_p) on pulse height (ΔE) (1st peak (■), 2nd peak (●), 3rd peak (▲), 4th peak (▼)).

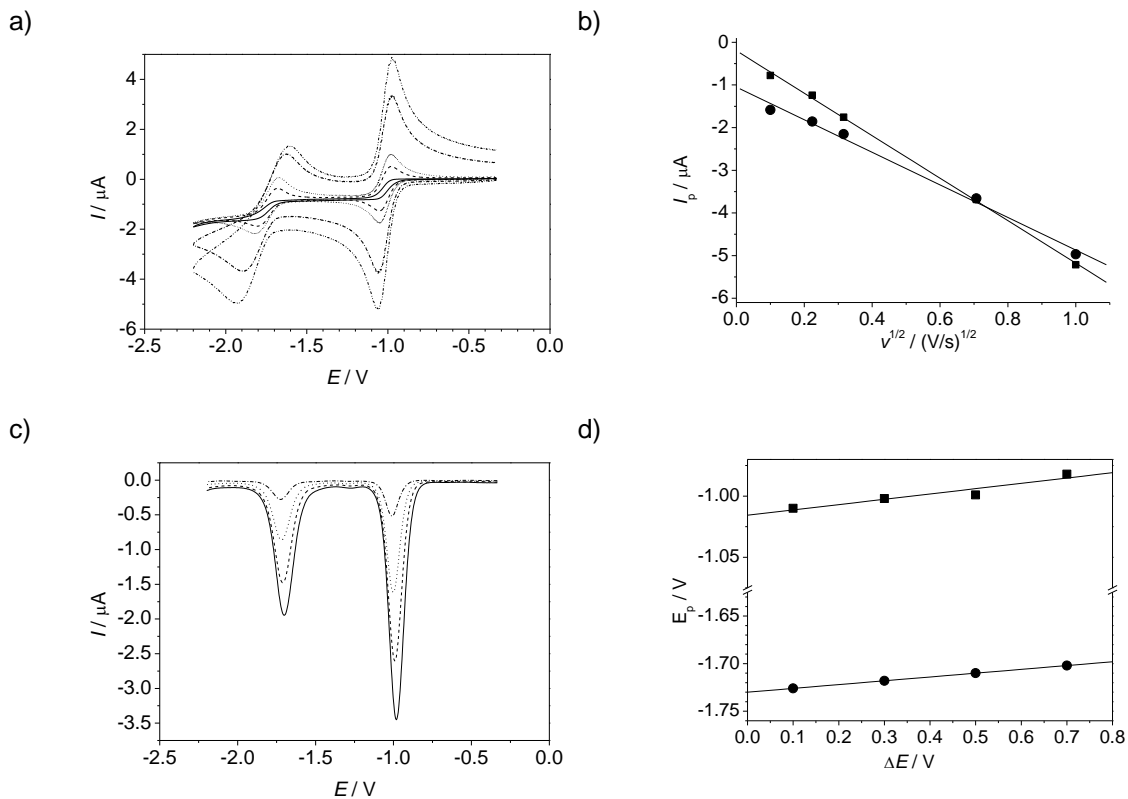
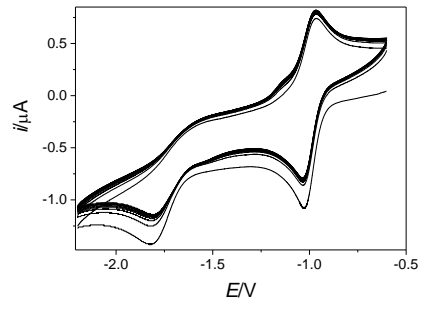
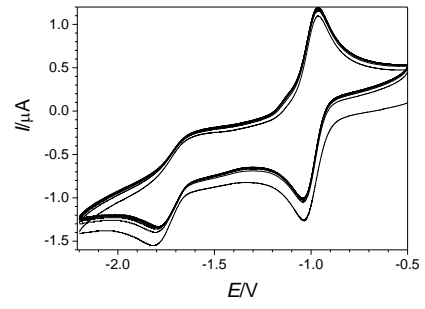


Figure S16. CV of **1** with $c = 1 \text{ mM}$. a) different scan rates (0.01 V/s (solid), 0.05 V/s (dashed), 0.1 V/s (dot), 0.5 V/s (dash-dot), 1.0 V/s (dash-dot-dot)), b) dependency of anodic peak potential (E_{pa}) on square root of scan rate ($v^{1/2}$) (1st peak (■), 2nd peak (●)), c) DPV with different pulse heights (0.07 V (solid), 0.05 V (dash), 0.03 V (dotted), 0.01 V (dash-dot)) and d) dependency of peak potential (E_p) on pulse height (ΔE) (1st peak (■), 2nd peak (●)).

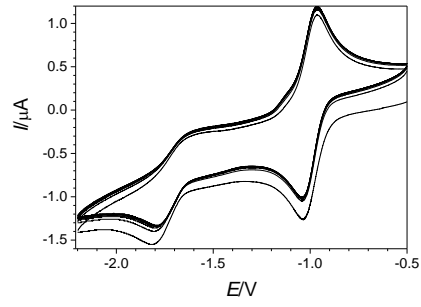
a)



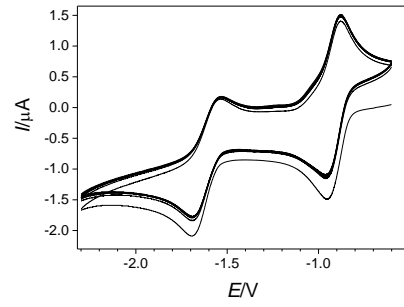
b)



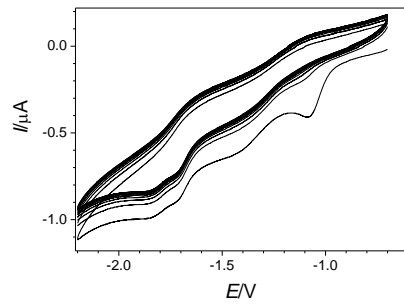
c)



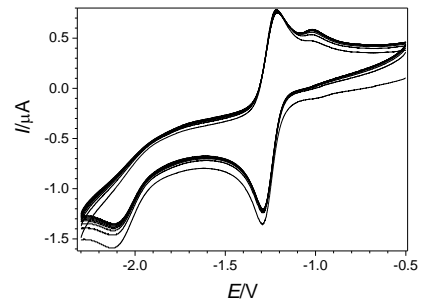
d)



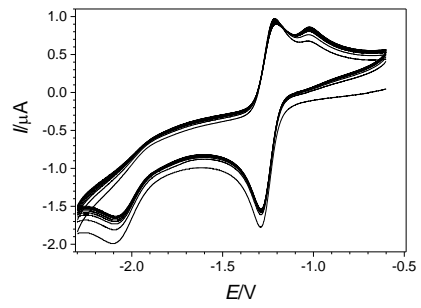
e)



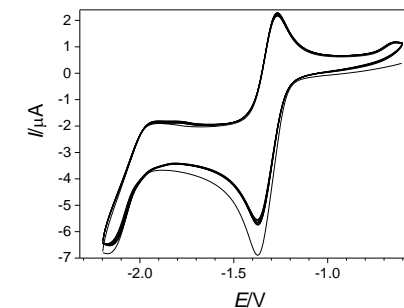
f)



g)



h)



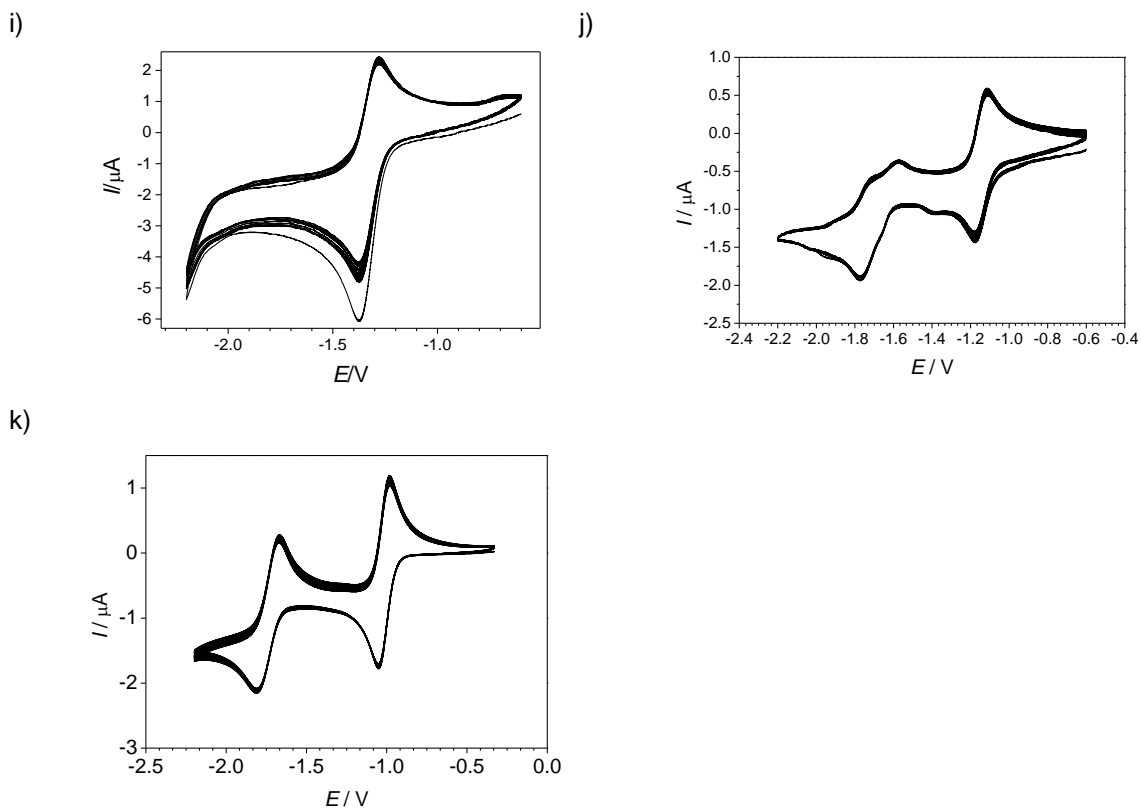


Figure S17. CVs with 20 cycles of (a) **5**, (b) **6**, (c) **7**, (d) **8**, (e) **9**, (f) **10**, (g) **11**, (h) **12**, (i) **13**, (j) **14**, (k) **1** at a scan rate of 0.1 V/s . (h) Comparison of first scan of each experiment for the synthesized azaathracenones **5-14**.

Cell cytotoxicity assay

The human tumor cell lines HeLaS3 and HepG2 were grown in incubation chambers at 37°C and 5% CO₂ in Dulbecco DMEM-medium (Invitrogen), to which 10% fetal calf serum were added. The cells were splitted every three days. Both cell lines were tested for infections with mycoplasma using the mycoplasma detection kit obtained from Roche Applied Sciences. For cytotoxicity tests, the cells were detached using trypsin and transferred into 96-well plates at a concentration of 1 million cells per ml and cultivated for 24 hours. After removal of the medium, different concentrations of the compounds to be tested were added in medium and the cells were incubated for 2 days. The amount of viable cells was determined using the Alamar Blue Assay.

All compounds to be tested were dissolved in the required amount of DMSO and then diluted with medium. In order to eliminate any effect associated with DMSO, the concentration of DMSO in the solutions used for incubation was kept below 0.5 %

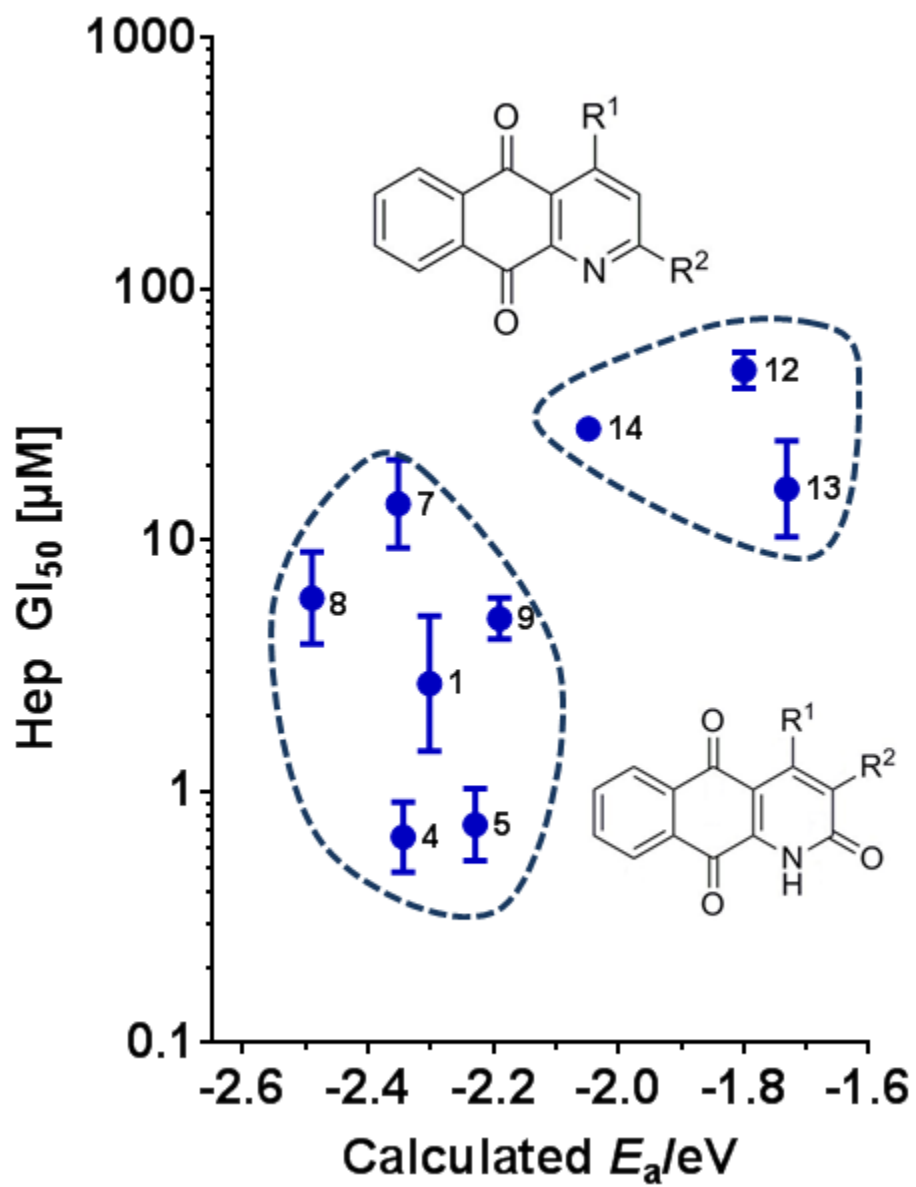


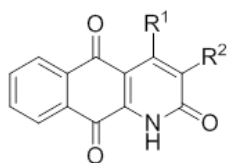
Figure S18. Correlation of Hep growth inhibition with electrochemical properties of marcanine A and synthetic derivatives.

Density functional calculations

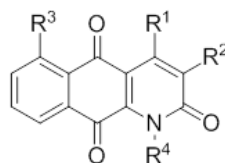
The structures of the neutral azaanthracenones were initially optimized at the B3LYP level of theory,²⁻⁵ using the 6-31+G(d) basis set. The nature of the resulting stationary point was determined by a subsequent frequency calculation. Refined energies were obtained by single-point calculations employing the larger 6-311+G(2d) basis set. Adiabatic electron affinities were calculated as the difference between the absolute energy of the neutral quinone and the radical anion. All calculations were done with the Gaussian 09 package of programs.⁶

Table S1. Summary of calculated adiabatic electron affinities E_a for various substituted non-natural azaanthraquinone derivatives and selected known natural products.

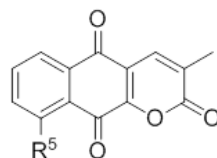
compound	E_a [eV]
15	-2.480
16	-2.573
17	-2.323
18	-2.685
19	-2.092
20	-2.358
21	-2.260
22	-2.279
23	-2.441
24	-2.491
25	-2.380
26	-2.316
27	-2.359
O ₂	-1.753
Marcanine B	-2.099
Marcanine D	-2.405
Dielsiquinone	-2.229
Lambertellin	-2.545



- | | | |
|----|----------------------------------|---|
| 15 | R ¹ = F | R ² = H |
| 16 | R ¹ = CF ₃ | R ² = H |
| 17 | R ¹ = NH ₂ | R ² = H |
| 18 | R ¹ = H | R ² = CF ₃ |
| 19 | R ¹ = H | R ² = NH ₂ |
| 20 | R ¹ = SMe | R ² = H |
| 21 | R ¹ = H | R ² = Me |
| 22 | R ¹ = H | R ² = SMe |
| 23 | R ¹ = H | R ² = F |
| 24 | R ¹ = H | R ² = Cl |
| 25 | R ¹ = H | R ² = Ph |
| 26 | R ¹ = H | R ² = C ₆ H ₄ -OMe |



- | | |
|---------------|--|
| Marcanine A | R ¹ = Me, R ² = H, R ³ = H, R ⁴ = H |
| Dielsiquinone | R ¹ = Me, R ² = OMe, R ³ = H, R ⁴ = H |
| Marcanine B | R ¹ = Me, R ² = OMe, R ³ = H, R ⁴ = Me |
| Marcanine D | R ¹ = Me, R ² = OMe, R ³ = OH, R ⁴ = H |



- | | |
|--------------|---------------------|
| 27 | R ⁵ = H |
| Lambertellin | R ⁵ = OH |

Figure S19. Constitution of various substituted azaanthraquinone derivatives and selected known natural products.

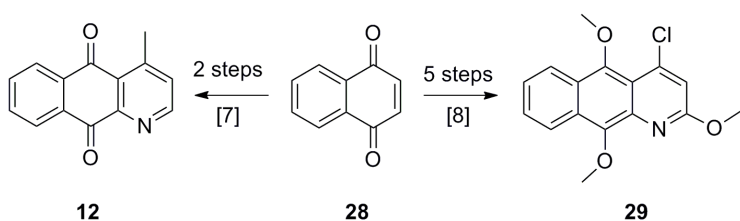
Overview of the multi-step synthesis

The multi-step synthesis of the marcanine A derivatives, used in this study is depicted in the schemes below (**schemes 1-3**).

Compound **12** was synthesized according to the published procedure by Bracher et al.⁷

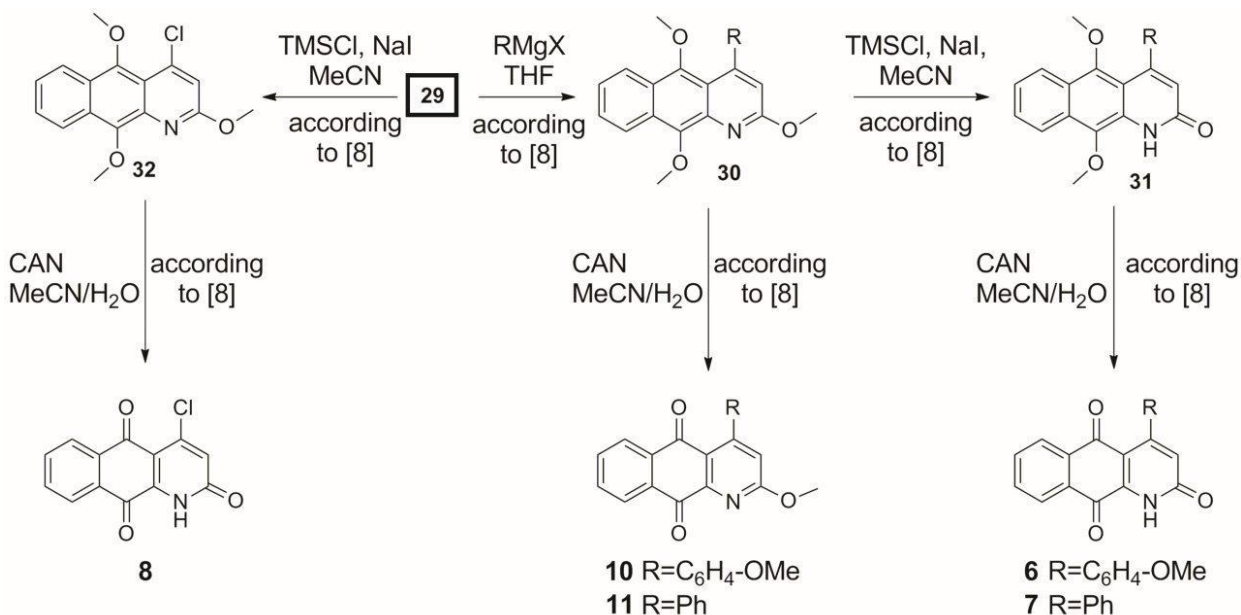
We have published the synthesis of the key building block **29** in 5 synthetic steps⁸, starting from the same commercially available starting material (1,4-naphthoquinone **28**).

Scheme 1.



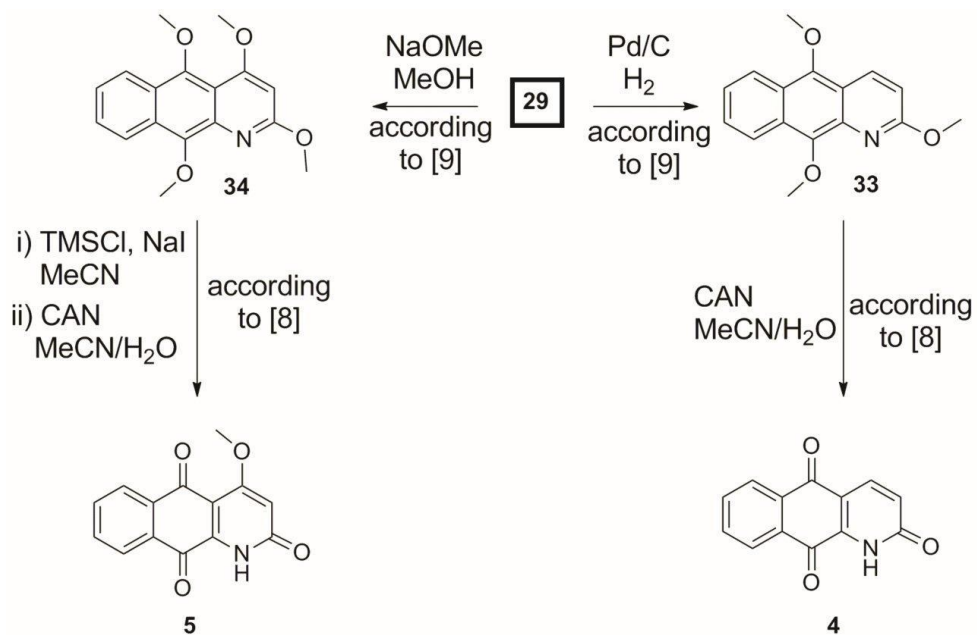
Following our published procedure⁸, compounds **8**, **10**, **11**, **6** and **7** were prepared from the key building block **29** (see **Scheme 2**).

Scheme 2.



Compounds **4** and **5** were synthesized and described in the PhD thesis by Steffen Lang⁹. An Overview of the reactions is given in **Scheme 3**.

Scheme 3.



Compounds **9**, **13** and **14** were prepared as described in the literature^{9, 10, 11}.

SUPPLEMENTARY REFERENCES

1. Gollas, B.; Kraub, B.; Speiser, B.; Stahl, H. *Current Separations* **1994**, *13*, 42.
2. Becke, A. D. *Physical Review A* **1988**, *38*, 3098.
3. Becke, A. D. *J. Chem. Phys.* **1993**, *98*, 5648.
4. Johnson, B. G.; Gill, P. M. W.; Pople, J. A. *J. Chem. Phys.* **1993**, *98*, 5612.
5. Lee, C.; Yang, W.; Parr, R. G. *Physical Review B* **1988**, *37*, 785.
6. Gaussian 09, Revision A.02, Frisch, M. J., et al., Gaussian, Inc., Wallingford CT, 2009.
7. F. Bracher, *Liebigs Annalen der Chemie* **1989**, *1*, 87.
8. S. Lang and U. Groth, *Angew. Chem. Int. Ed.* **2009**, *48*, 911.
9. S. Lang, PhD Thesis, Synthese und biologische Evaluierung von Azaanthracenonen, Cuvillier Verlag Göttingen, 2009, ISBN: 9783869551289.
10. W.S. Johnson, F. J. Mathews *J. Am. Chem. Soc.* **1944**, *66*, 210.
11. K.T. Potts, D. Bhattacharjee and E.B. Walsh, *J. Org. Chem.* **1986**, *51*, 2011.